Research Article

Nano Research
2023, 16(8): 11326–11333

ISSN 1998-0124 CN 11-5974/O4
https://doi.org/10.1007/s12274-023-5934-1

Graphene-coated conductive probes with enhanced sensitivity for nanoIR spectroscopy

Yu-Jiao Xia-Hou, Xu-Cheng Li, En-Ming You, Hong-Peng He (✉), Jun Yi (✉), Jun-Rong Zheng, Hai-Long Wang, Hai-Xin Lin (✉), and Zhong-Qun Tian

State Key Laboratory of Physical Chemistry of Solid Surfaces, College of Chemistry and Chemical Engineering, School of Electronic Science and Engineering, Collaborative Innovation Center of Chemistry for Energy Materials (iChEM), Innovation Laboratory for Sciences and Technologies of Energy Materials of Fujian Province (IKKEM), Xiamen University, Xiamen 361005, China

Received: 30 April 2023 / **Revised:** 11 June 2023 / **Accepted:** 14 June 2023

ABSTRACT

Nano-infrared (nanoIR) probes play a crucial role as nano-mechanical sensors and antennas for light absorption and emission, and their testing performance is critically dependent on their optical properties and structural stability. Graphene-coated dielectric probes are highly attractive for enhancing light–matter interactions and integrating IR photonics, providing a broadband optical response and strong electromagnetic field. However, achieving continuous single-layer graphene growth on non-planar and non-single crystalline dielectrics is a significant challenge due to the low surface energy of the dielectric and the large difference in size between the probe tip, cantilever, and substrate. Herein, we present a novel method for the growth of high-quality and continuous graphene with good conductivity on non-planar and amorphous dielectric probe surfaces using manganese oxide powder-assisted short time heating chemical vapor deposition. The resulting graphene-coated dielectric probes exhibit an average IR reflectance of only 5% in the mid-IR band, significantly outperforming probes without continuous graphene coating. Such probes can not only effectively transduce the local photothermal sample expansion caused by the absorption of IR laser pulses, but also effectively scatter near-field light, which is 25 times stronger than the commercial metal-coated probes, and have advantages in the application of nanoIR sensing based on atomic force microscope-based infrared (AFM-IR) spectroscopy and infrared scattering scanning near field optical microscopy (IR s-SNOM) principles. Furthermore, our graphene growth method provides a solution for growing high-quality graphene on the surfaces of non-planar dielectric materials required for integrated circuits and other fields.

KEYWORDS

graphene-coated, nano-infrared (nanoIR) spectroscopy, atomic force microscope-based infrared (AFM-IR), infrared scattering scanning near field optical microscopy (IR s-SNOM), conductive probe

1 Introduction

Associating spatially resolved chemical information at the nanoscale with reproducible and highly sensitive patterns of tightly packed nanostructures remains a challenge in surface science [1, 2]. Tip-enhanced nanoscale infrared (nanoIR) spectroscopy [3, 4] combining the advantages of scanning probe microscopy (SPM) and IR spectroscopy breaks through the optical diffraction limit, and gives outstanding contribution to the research on crystal electronic structure visualization [5], chemical composition [6], carrier diffusion imaging [7], and charge transfer and other processes [8]. The probe can effectively excite and transmit signals such as light scattering fields, sample thermal expansion, and photo-induced force in the nanometer gap between the probe tip and the sample, which is the key to achieving high-sensitivity nanoIR spectroscopy [9].

Nano-shelled Au and platinum-iridium (PtIr) probes, which are known to exhibit certain near-field enhancement in the IR region, have usually been used for nanoIR spectra acquisition and imaging. However, the metal-coated probes exhibit conductor-like properties in IR band, so that the electric field penetration and high spatial confinement vanish [10]. Moreover, metal layers are not wear-resistant and are prone to shedding, limiting their application in nanoIR-associated electrical or electrochemical under contact mode. Interestingly, the electric fields generated by plasmon waves at the top and bottom surfaces are coupled with the reduction of a conductor's thickness from bulk to monoatomic [11, 12], which in turn drives charge and field oscillations simultaneously. Graphene with single atomic layer thickness has a dispersion relation far away from light, which enables achieving a significantly lower group velocity at IR frequencies and much greater subwavelength confinement than bulk metal layers, and produces stronger light–matter interaction [13]. Surface plasmon polariton (SPP) waves can be naturally confined and propagated on curved graphene surfaces with little radiation losses at the curved part [14]. In addition, the high mobility of graphene translates to a small plasmon damping rate, which leads to a longer plasmon propagation length and plasmon lifetime. Therefore, graphene-coated dielectric probes are one of the best candidates for obtaining better IR near-field enhancement

Address correspondence to Hai-Xin Lin, haixinlin@xmu.edu.cn; Hong-Peng He, hphe@xmu.edu.cn; Jun Yi, junyi@xmu.edu.cn

and improving the sensitivity of nanoIR spectra [15].

Usually, SPM probes are composed of a tip with a nanoscale curvature radius, a micrometer-scale cantilever, and a millimeter-scale base, spanning a wide feature size range. Coating continuous single-layer graphene (SLG) on such non-planar dielectric probes' surfaces is a huge challenge. Several research strategies have been proposed to solve this problem [16]. The simplest method is to directly drop the graphene dispersion onto the probe surface [17], but it is difficult to obtain large-area wrinkle-free SLG on the tip [16]. An effective method is to pre-grow SLG and then wet-transfer it onto the probe surface [18, 19]. However, wet chemical method may promote the additional extrinsic defects and residual pollution, thus distorting the information of the analyte of interest. In contrast, direct growth of graphene on the probe surface is a fast, efficient, and mass-producible clean method. In addition to catalytic metallic foils (such as Cu, Ni, and Fe), single crystal dielectric surfaces such as Ge [20] and SiC can also achieve high-quality growth of graphene. However, more stringent requirements (higher temperature or longer reaction time) are imposed on the growth conditions and the crystal faces of dielectric materials, due to the low surface energy [21]. However, it is difficult to coat the single crystal dielectric shell on the probe surface because of its large size span, which in turn makes the coating of continuous SLG even more challenging. Low pressure chemical vapor deposition (LPCVD) method [22] was reported to be an effective way to realize graphene growth on the surface of photonic crystal fiber, while with large amounts of defects that would affect the electronic and optical properties.

Herein, a novel manganese oxide powder-assisted short time heating chemical vapor deposition (MnO-STCVD) method [23] was developed to achieve high quality continuous monolayer graphene coating on amorphous and non-planar probe surfaces. This method is highly inclusive of the basic morphology of the probe, such as tip shape and height, cantilever shape, and spring constant ($>$ 0.3 N/m), and the curvature radius of the prepared tip is constantly less than 100 nm. Compared with the commercial metal-coated probe, this probe shows a very low reflectivity in broadband IR region. Thus, the as-prepared probe shows greater sensitivity in local molecular vibrations detection applied to atomic force microscopy-infrared (AFM-IR) spectroscopy. Moreover, the probe applied to scattering-type scanning near-field optical microscopy (s-SNOM) enhanced the scattering of background light by an order of magnitude compared to that of the metal-coated probe. Thanks to the complete coating of graphene, the probe has good conductivity and can be used as a candidate for wear-resistant conducting-probe and electrochemical nanoIR probe.

2 Experimental

2.1 Materials

All reagents were purchased and used without further purification. Probes: SCANASYST-AIR probes and SCM-PIT-V2 probes were purchased from Bruker; 3XC-NN probes were purchased from OPUS; Arrow NCPt probes were purchased from NanoWorld; PPP-NCSTAu probes and PPP-NCH probes were purchased from Nanosensors; and HQ:NSC14 probes were purchased from Mikromasch. MnO_2 target (99.9%) was purchased from NanChang Hanchen New Materials Technology Co., Ltd. Calibration grating TGQ1 was purchased from NT-MDT Company (Russia). High purity argon (Ar, 99.999%), hydrogen (H_2, 99.999%), and methane (CH_4, 99.999%) were purchased from Linde gases Co., Ltd. Water used in all experiment was Milli-Q ultrapure water (18.2 MΩ·cm).

2.2 Preparation of graphene-coated dielectric probes

2.2.1 *Probes cleaning*

(a) Commercial SPM probes were washed in acetone for 10 min, ethanol for 10 min, and ultrapure water for 10 min, and then blow dried with nitrogen gas.

(b) Metal-coated probes were first thoroughly cleaned with *Aqua Regia* solutions consisting of HCl (37%) and HNO_3 (65%) with a volume ratio of 3:1, followed by thorough rinsing with H_2O and then blow drying with nitrogen gas. Caution: *Aqua Regia* solutions are dangerous and must be used with extreme care and never stored the solutions in closed containers.

2.2.2 *Growth of Mn_xO_y layer on tip side by magnetron sputtering*

The cleaned probes were placed under vacuum. 100 nm Mn_xO_y layers were grown on the surface of tip side under vacuum (10^{-4} Pa) at room temperature using a MnO_2 target. The power was 50 W. The growth of dielectric layer was conducted using a magnetron sputtering machine (Chengdu Vacuum Machinery Factory JC-500-3/D).

2.2.3 *Growth of graphene layer on tip sides by MnO powder-assisted short time heating chemical vapor deposition*

The probes were then placed retrogradely into a quartz boat, and the MnO powder was positioned under the probes. The distance between the probes and transition metal carbide (TMC) powder was set as 0.3 to 3 mm. 3%–13% methane (mixed with argon and hydrogen) was used as carbon feedstock and the chemical vapor deposition (CVD) reaction was carried out at about 1000 °C for 3–10 min.

2.2.4 *Oxygen plasma etching*

The graphene layer on the back side of the tip of the probes was treated by the oxygen plasma for 5 s, 50 W.

2.2.5 *Fluorine plasma etching*

The Mn_xO_y layer on the back side of the tip of the probes was treated by the fluorine plasma for 50 s, 400 W.

2.2.6 *Reflective layers growth*

The reflective layers were metalized by electron beam evaporation of 25 nm Au with a 5 nm Cr adhesion layer on the back side of cantilevers.

2.3 Micro-IR reflectance spectra of probe

The 20 μm × 20 μm square collection aperture was used for the micro-IR reflectance spectra of probe measurements. The reflectance spectra of the probes were defined as the signal intensities reflected from the tip area divided by those from a background taken at a gold film at room temperature. The incident and collected light were unpolarized light. Each spectrum was acquired by averaging 64 spectra with a 4-cm^{-1} spectral resolution.

2.4 Characterization

Scanning electron microscopy (SEM) images were acquired with a Hitachi S-4800 field emission scanning electron microscope. TEM images were obtained on FEI Technai F30 microscope at 300 kV. Raman spectroscopy was performed using a Renishaw RM1000-Invia with laser excitation wavelength of 532 nm (2.33 eV). The phase structure of the as-prepared probes was analyzed by using X-ray diffraction (XRD) on a Rigaku Ultima-IV system with Cu Kα radiation (λ = 1.5406 Å). Micro-Fourier transform infrared (FTIR) spectra were measured by an infrared micro-spectrometer

(Thermo Scientific Nicolet iN10 (USA)). s-SNOM data was acquired using a commercialized neaSNOM system (neaspec, GmbH). AFM-IR spectra and images were acquired by a homemade system based on Dimension ICON (Bruker). The electrical conductivity of probes was measured using an AFM (Dimension 3100, Veeco) under tapping mode at a slow scanning rate. Electric properties of probes were tested with the precision semiconductor parameter analyzer (Tektronix 4200A-SCS source meter) and low temperature vacuum probe station (Lake Shore Cryotronics, Inc CRX-6.5K).

3 Results and discussion

3.1 Graphene-coated dielectric probes prepared by MnO-STCVD method

In this work, graphene-coated dielectric probes are used for nanoIR applications based on AFM-IR or s-SNOM, applied to contact mode, tapping mode, and peak-force tapping mode, while also having electrical testing functions. Such probes are grown using typical AFM probes as templates: The silicon-based probes (Fig. 1(a_1)) were first thoroughly cleaned. And then the dielectric layers (say, 100 nm Mn_xO_y layer, Fig. 1(a_2)) with small grain size were grown on the tip side of probes, exploiting a low-power impulse magnetron sputtering deposition system (Fig. S1 in the Electronic Supplementary Material (ESM)). The high flatness of Mn_xO_y layers contributes to the continuous growth of the graphene shell. Highly uniform SLG (Fig. 1(a_3)) was coated onto the Mn_xO_y layers by MnO-STCVD method as revealed by SEM images (Fig. 1(b)) and Raman data (Fig. 1(c)). The as-prepared graphene-coated dielectric probes remain smooth surface (Fig. 1(b) and Fig. S2 in the ESM) with a nominal radius of curvature for the tip of less than 100 nm (inset in Fig. 1(b)), even the distances between the tip and cantilever up to micron size or even submillimeter. Although the radius of curvature of the probe is significantly increased by the coating of the Mn_xO_y layer (Fig. S2 in the ESM), the graphene-coated dielectric probe still maintains the same spatial resolution as the commercial PtIr probe with the same cone angle (Fig. S3 in the ESM). To characterize the quality of graphene on the probe surface, Raman spectra were collected from the probe tip and cantilever. As shown in Fig. 1(c), regardless of whether it was the probe tip or cantilever position, the intensity of the two-dimensional (2D) band relative to the G band ($I_{2D/G}$) is greater than 3 (Table S1 in the ESM), which demonstrates the monolayer graphene with sp^2 hybridized carbon atoms [24]. The D peak was extremely low, indicating that graphene had few defects and was conducive to amplifying 2D [25].

The spring constant (k) of the probe cantilever is crucial for controlling the interaction between the probe tip and sample surface. Therefore, we further verify the effectiveness and universality of MnO-STCVD method by using probes with cantilevers of different shapes and k. Continuous SLG was successfully grown on the surfaces of the probes with k ranging from 0.4 to 42 N/m (Fig. 1(d)–1(f), and Figs. S4 and S5 and Tables S2 and S3 in the ESM). The growth of the Mn_xO_y layer would cause cantilever bending when the k is less than 9 N/m, which makes it difficult to achieve the application for beam deflection based on a four-quadrant photoelectric detection system (Fig.

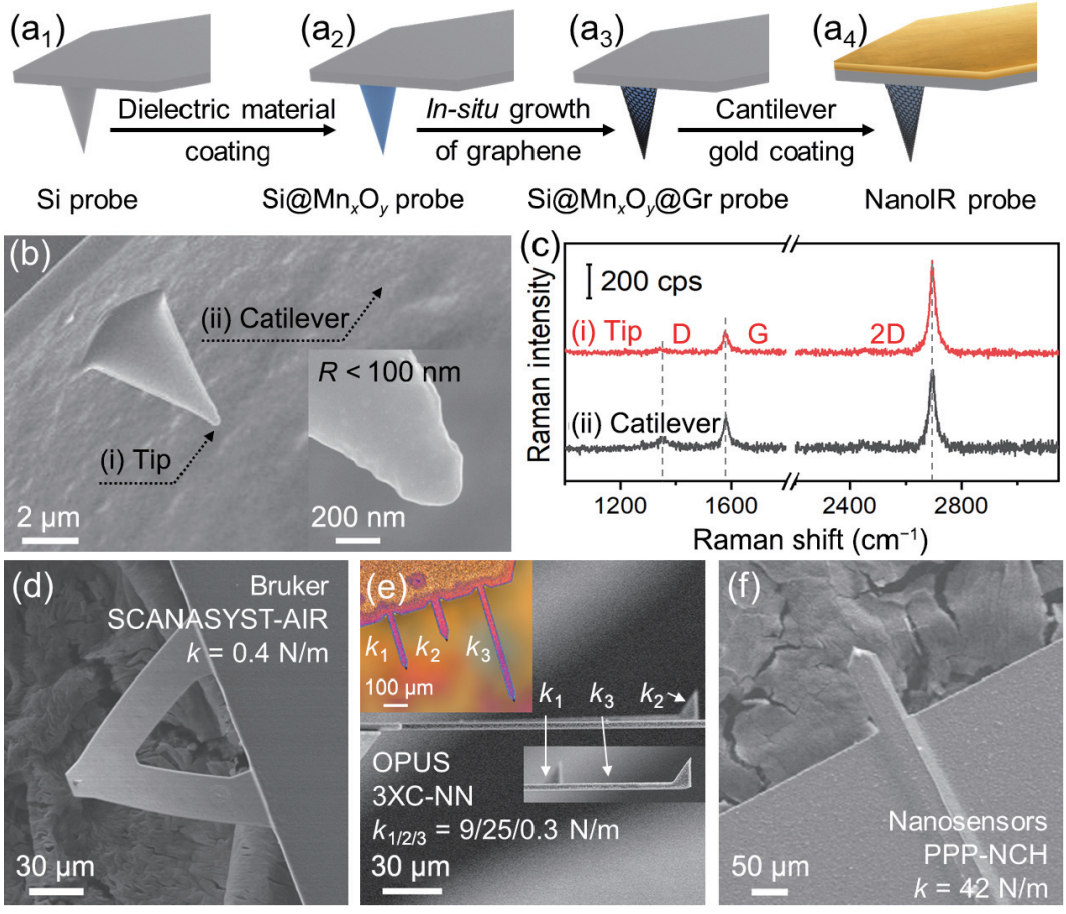

Figure 1 (a) Schematic representation of the preparation of graphene-coated nanoIR probe. (b) SEM images of Si@Mn_xO_y@Gr probe. The inset in (b) shows the radius of curvature of the tip. (c) Typical Raman spectra of (i) tip and (ii) cantilever; black arrows in (b) represent the positions of Raman spectra collection. SEM images of the final conductive nanoIR probe with different geometry and k: (d) triangular cantilever, k = 0.4 N/m (model SCANASYST-AIR, Bruker); (e) rectangular cantilever, $k_{1/2/3}$ = 9/25/0.3 N/m (model 3XC-NN, OPUS). The inset in upper left of (e) is optical photo of the top view of the probe. The inserted SEM image is the k_1 and k_3 cantilever of probe extended from (e); and (f) rectangular cantilever, k = 42 N/m (model PPP-NCH, Nanosensors).

S5(b) in the ESM). Interestingly, during the growth of graphene using the MnO-STCVD method, this cantilever bending phenomenon disappeared, which may be attributed to thermal release of partial stress. In addition, for probes with a k less than 0.5 N/m, the dip angle of the cantilever can be further balanced by adjusting the thickness of the metal reflective layer on the back of the cantilever (Fig. S5(c) in the ESM). The average sum value of the photodetector of AFM can reach 9.5 by using the graphene-coated dielectric probe, which is higher and more stable than commercial probes (Tables S2 and S3 in the ESM), and would be beneficial to achieve higher sensitivity of SPM-based detection. These results show that MnO-STCVD method has potential wider universality and repeatability compared with liquid-phase graphene film method and transfer or mold-assisted transfer SLG method. Moreover, the preparation of such probes in large batches is possible by this method.

One great concern about the growth of the graphene-coated dielectric probes is whether the graphene can be homogeneously distributed on the steep probe tip surface with smaller radius of curvature, as the pressure distribution of gas flow in windward and leeward of tip have huge variability and the low surface energy of the dielectric. The continuous growth of SLG cannot be achieved by the direct CVD method (Fig. S6(a) in the ESM), and there will be a large number of defects on the graphene surface. To solve this problem, the probes are fixed to the surface of a large size silicon wafer to improve the uniformity of gas flow. However, the as-grown graphene is still not immune from structural defects (Fig. S6(b) in the ESM). Thus, more precise growth dynamics control is further required for continuous growth of SLG on the surface of non-planar dielectric.

It is found that parts of TMCs (Fig. 2(a)) display excellent heterogeneous catalytic activities, especially for dehydrogenation and aromatization of hydrocarbons [26–28]. The previous work reported that MnO can be easily converted to manganese carbide (Mn_7C_3) in CH_4 atmosphere [29], and is easy to further grow high quality SLG by STCVD method [23]. Bearing these in mind, we developed a subspace of finite field MnO-STCVD method to realize the graphene coating. Firstly, MnO microwires (MnO MWs) were tiled in quartz boat at the center of furnace as assist-growth source; then, the Mn_xO_y-coated probes fixed to silicon chips were placed above the assist-growth source or upon behind the gas-flow (Fig. 2(b) and Fig. S7 in the ESM). The defects and the number of graphene layers could be effectively controlled by the growth parameters, including carbon source, gas flow and pressure, the pyrolysis temperature, and the concentration and position of the promotors. When exposed to reducing gases, the MnO MWs and Mn_xO_y layer would firstly generate oxygen vacancies with a high density at the high temperature of 1000 °C. Then, the Mn–O bonding would be *in-situ* replaced by Mn–C bonding via carburization. The Mn atoms with high catalytic activity and carbon affinity of the dominant crystallographic plane of Mn_3C_7 (211) surface promoted the dehydrogenation of CH_4 [29] to form the $–CH_3$ radical intermediate. Some $–CH_3$ radicals may release from the Mn sites, and others may undergo further dehydrogenation.

At defined conditions (see Section 2 for details), SLG can be synthesized by simply tuning the distance between the probe and MnO MWs powder (Figs. 2(b)–2(d)). As the distance (h_{Tip} in Fig. 2(d)) gradually increases from (i) 0.44 to (ii) 0.73, (iii) 1.07, (iv) 1.47, and (v) 2.57 mm, there is a gradual transformation of the grown graphene on the probe tip from multilayer ((i) and (ii)) to monolayer ((iii) and (iv)) then to multilayer (v), as illustrated in Fig. 2(e). It is also found that the surface defect density of graphene gradually increases as the number of graphene layers increases (Fig. S8 and Table S4 in the ESM). When the distance was controlled between 1.07 and 1.47 mm, Raman spectra of graphene showed monolayer thickness and low defect density, which means that the proposed method has a relatively wide monolayer graphene growth window in the height range of at least 400 μm, fully covering the tip length of current AFM, nanoIR, and even terahertz probes [30]. The elemental composition of the probes before and after graphene coating was obtained by energy dispersive X-ray spectroscopy (EDS) analysis (Table S5 in the ESM). Meanwhile, the structural characterizations of graphene-

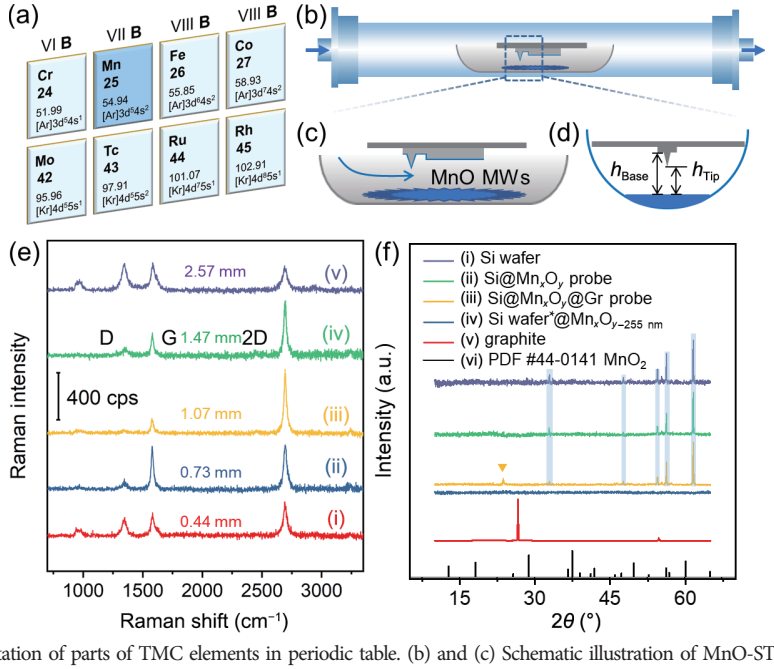

Figure 2 (a) Schematic representation of parts of TMC elements in periodic table. (b) and (c) Schematic illustration of MnO-STCVD system for robust graphene growth on dielectric probe; arrows designate the direction of gas-flow. (d) Side view of the height between the assisted powder and tip or base of probe. (e) Raman spectra of graphene at different height differences: (i) 0.44 mm, (ii) 0.73 mm, (iii) 1.07 mm, (iv) 1.47 mm, and (v) 2.57 mm. (f) XRD patterns of n-doped Si wafer ((i) violet line), Si@Mn_xO_y tip ((ii) green line), Si@Mn_xO_y@Gr tip ((iii) yellow line), Si@$Mn_xO_{y-255\ nm}$ films ((iv) bule line), and graphite ((v) red line, about 10 layers of graphene). The blue transparent lines in (f) indicate the correspondence of the characteristic peaks of Si wafer with the ones observed in each probe. The Mn_xO_y film in ((f)(iv)) was prepared on a zero-diffraction Si wafer*. The standard PDF card ((f)(vi)) is PDF #44-0141, MnO_2.

coated dielectric probes were further assessed by XRD. The XRD pattern between 30° and 65° showed that the dielectric coated probes (Fig. 2(f)(ii)) and graphene-coated probes (Fig. 2(f)(iii)) bear the similar features with Si wafer (Fig. 2(f)(i)), and provided evidence of the amorphous nature of Mn_xO_y layer (Fig. 2(f)(iv)), even if the thickness of the Mn_xO_y layer was increased to 255 nm (Fig. 2(f)(iv), PDF #44-0141, MnO_2). Figure 2(f)(iii) shows a sharp peak at 2θ = 23.8°, which is smaller than the typical peak of graphite (about 10 layers of graphene) at 26.5° (Fig. 2(f)(v) and Fig. S9 in the ESM) [31], when bilayer graphene is coated on the probe (Fig. 2(e)(v)). This observation suggests the presence of residual stress in the non-planar graphene coating [23, 32].

3.2 High conductivity of the graphene-coated Mn_xO_y probes

To confirm the continuity of SLG on the graphene-coated Mn_xO_y probes, the electrical conductivity between the cantilever and base was measured in a two-point probe system. Two gold probes were carefully placed on the probe base (Figs. 3(b)(i) and 3(c)(i)) and cantilever (Figs. 3(b)(ii) and 3(c)(ii)) with a distance larger than 70 μm. Then, the electrical bias was applied using a semiconductor analyzer (the lower inset in Fig. 3(a)). The linear current–voltage (*I*–*V*) curve indicates the ohmic-like contact between the surface of probe and the metal probes. The average resistance of graphene-coated Mn_xO_y probes is about 20 Ω (red line in Fig. 3(a)). The resistance was reduced by 12 orders of magnitude compared to the Mn_xO_y-coated probe without graphene coating (black line and the upper inset in Fig. 3(a)). Further, the graphene-coated Mn_xO_y probes were mounted on a conductive AFM (C-AFM) for practical applications. A schematic illustration of the experimental configuration for the C-AFM measurements is shown in Fig. 3(d), where all data acquisition was done at room temperature in air.

The resistance of the system was tested by commercial conductive gold-coated probe and graphene-coated dielectric probe, respectively, with a flat gold film of 100 nm as the conductive substrate. A voltage was applied to the gold film so that a current flowed between the tip and the sample, and this current was recorded by a current amplifier. The electrical characteristics of each conducting-probe could be well quantified by measurements of the *I*–*V* curves, as exemplified in Fig. 3(e) by the comparison of a typical *I*–*V* curve obtained from the gold- (black line in Fig. 3(e)) or graphene-coated (red line in Fig. 3(e)) tip. When the bias voltage is set to plus or minus 0.15 V, the resistances of the gold- and graphene-coated probes test system are 40 and 1000 μΩ, respectively. These C-AFM measurements clearly indicated that the good conductivity of graphene-coated probes can be used for sample conductivity measurement, but the conductivity of graphene-coated probes is 25 times less than that of commercial metal-coated probes.

3.3 NanoIR sensing with high sensitivity by using graphene-coated dielectric probes

Figure 4 illustrates the IR reflectance spectra of different types of probes. The Mn_xO_y-coated probes (Fig. 4(ii)) have a high IR reflectance in the mid-IR range (from 1500 to 4000 cm^{-1}), which is similar to metal-coated probes (Figs. 4(iii) and 4(iv)), with the average reflectance of 65%–80%. We observed that a significantly reduced reflectance spectrum in the broadband IR appears after SLG coating, and the average reflectance was just about 5% (Fig. 4(i)), which means that the probe has strong absorption and/or scattering to mid-IR light. For comparison, metal and dielectric probes partially coated with multilayers of graphene oxide (GO) were prepared and shown in Fig. S10 in the ESM with an average reflectivity of about 37% (Figs. 4(v) and 4(vi)). These results indicate that the IR reflectance of continuous SLG-coated dielectric probes is significantly lower than that of multilayer discontinuous GO-coated dielectric or metal probes. Note that there are regular fluctuations in the reflection spectra of the tip with a 20 μm × 20 μm aperture because the micro-IR with small aperture interferes with the non-planar structure. This can be solved by hardware [33] such as high angle incident objective lens, large-size aperture, or other algorithm [34] correction techniques.

AFM-IR spectroscopy transduces the photothermal expansion of the sample through the tip of nanoIR probes, measures local thermal expansion of sample under IR laser absorption, and thus maps material absorption over a range of wavenumbers (Fig. 5(a)). Polymethyl methacrylate (PMMA) is a frequently used model molecule in nanoIR research owing to its well-characterized vibrational modes and strong IR absorption. An IR laser can induce a larger local thermal expansion of the PMMA film when excited by 1734.4 cm^{-1}, which matches to the wavenumber of C=O stretching vibration. Schematically, the lower cantilever spring

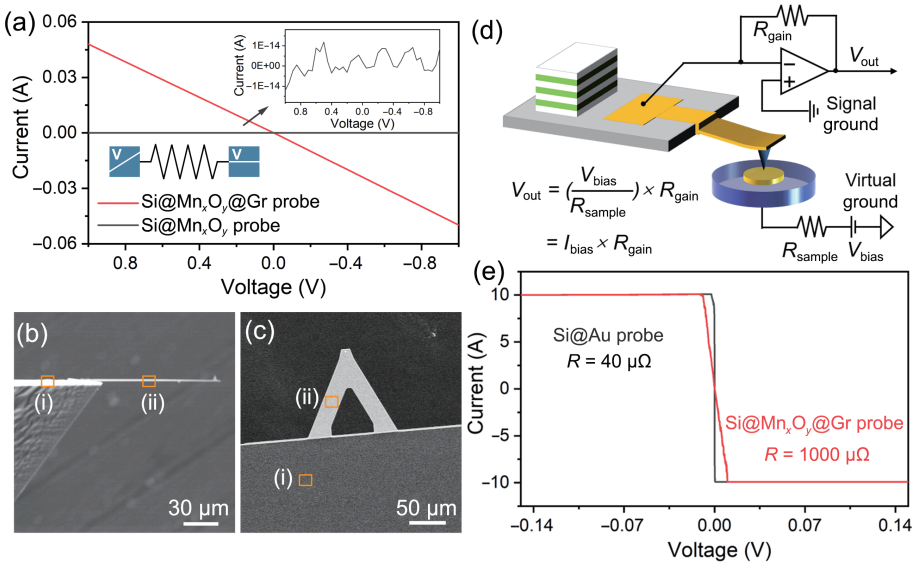

Figure 3 Electrical conductivity of graphene-coated Mn_xO_y probes. (a) *I*–*V* curves of Si@Mn_xO_y@Gr probe (red line) and Si@Mn_xO_y probe (black line) between (b)(i) base and (b)(ii) cantilever, the lower inset is the schematic illustration of test principle, and the upper inset is the magnified image the *I*–*V* plot of Si@Mn_xO_y probe. (b) Cross-section and (c) top-view SEM images of the tested graphene-coated dielectric probe. (d) Schematic diagram of the experimental setup for the C-AFM measurements. (e) Electrical performance of graphene-coated dielectric probe (red line) and commercial gold-coated probe (black line, model PPP-NCSTAu).

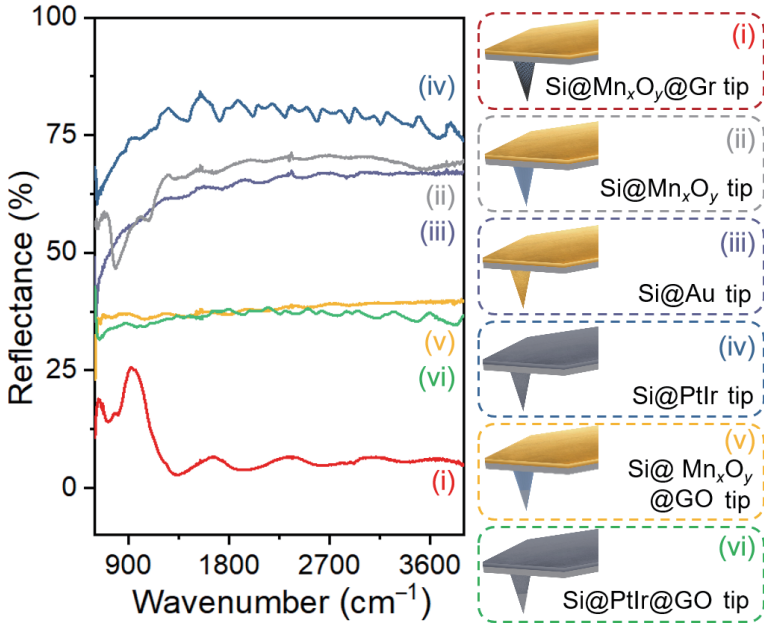

Figure 4 IR reflectance spectra and corresponding schematic picture of different tips: (i) Si@Mn_xO_y@Gr tip; (ii) Si@Mn_xO_y tip; (iii) Si@Au tip; (iv) Si@PtIr tip; (v) Si@ Mn_xO_y @GO tip; and (vi) Si@PtIr@GO tip.

constant of the probe enhances the sensitivity of the detection of the molecule's vibrational properties under similar condition.

For a fair comparison, homemade dielectric-coated probes (Si@Mn_xO_y probes, Fig. 5(b)(i)) and gold-coated probes (Si@Au probes, Fig. 5(b)(ii)) were fabricated with the same spring constants (42 N/m) as the SLG-coated dielectric probes (Si@Mn_xO_y@Gr probes, Fig. 5(b)(iv)). The vibration signal cannot be distinguished from the background noise using dielectric-coated probes (Fig. 5(b)(i)). In striking contrast to the dielectric probes, the nanoIR signal was significantly improved when the same specifications (k = 42 N/m) graphene-coated dielectric probe was used (Fig. 5(b)(iv)). The enhancement is higher than that of both the gold-coated probes (k = 42 N/m) and even commercial gold-coated probes with a lower spring constant (Fig. 5(b)(iii), k = 5 N/m), thus further confirming the advantage of the photothermal transduction performance of the graphene-coated dielectric probes. In addition to exhibiting a sensitive nanoIR sampling spectrum, graphene-coated probes also demonstrate significantly enhanced sensitivity for nanoIR imaging. We conducted IR absorption mapping on polystyrene (PS) films at a frequency of 1493 cm^{-1}, which corresponds to the benzene ring stretching vibrations (Fig. S11 in the ESM). The findings reveal that graphene-coated probes exhibit superior chemical imaging sensitivity compared to metal-coated probes, even when the laser power is reduced by 7 times.

Near-field scattering ability of probes to IR light was verified using a commercial neaSNOM system (neaspec GmbH, Germany) based on s-SNOM. In practice, a laser is focused at the intersection of the tip and the sample, and an enhanced localized electric field is formed at the tip. When the enhanced field interacts with the evanescent field from the surface plasmon resonance (SPR) of the sample, the light scattered to the far-field detector carries information about the local optical properties of the sample (Fig. 5(c)). Here, blank Si wafer was set as a sample to investigate the scattering intensity of different probes to background light source (Fig. 5(d)). Apart from the tip coating, all other conditions were kept identical. The background light scattering intensity enhanced by SLG-coated probes (Fig. 5(d)(ii)) was found an order of magnitude stronger than PtIr-coated probes (Fig. 5(d)(i)). The greatly enhanced molecular vibration and light scattering intensity by graphene-coated probe can be qualitatively understood by the strong absorption and scattering of the mid-IR light, which could also be evidenced by the low reflectance in the whole mid-IR band (Fig. 4(i)). In addition, the graphene-coated probes show good environmental stability after storage in air for 18 months, and good structural stability after the contact mode test (Fig. S12 in the ESM).

3.4 Outlook for the next-generation nanoIR probes

In the above experiments, we demonstrate that the graphene-coated dielectric probe with curvature radius of 100 nm has excellent near-field enhancement performance, which in turn exhibits better performance than commercial metal-coated probe in nanoIR test. Since the radius of curvature of the tip determines the spatial resolution of chemical imaging, deep sub-wavelength resolution can be achieved at IR frequency. Therefore, the graphene-coated dielectric probes with smaller radius of curvature were realized by further regulating the growth parameters. On the one hand, the curvature radius of the probe can be controlled to less than 75 nm by reducing the thickness of the Mn_xO_y layer on the surface of probe (Fig. S13 in the ESM). However, if the Mn_xO_y layer is too thin (say, less than 30 nm), severe dielectric atomic migrations are prone to occur at high temperatures, resulting in discontinuous growth of graphene. The other method is to provide a higher concentration of carbon source and a longer growth time (Figs. S13(b) and S13(c) in the ESM). Mn_xO_y layers can catalyze the growth of carbon nanotube (CNT)-like structures on the probe surface along with the carbon source supplied by surface diffusion (Fig. S13(d) in the ESM). The internal Mn_xO_y keeps an amorphous structure before and after the growth. The curvature radius of probes with the CNT-like structures can be controlled between 10 and 50 nm.

Nevertheless, the CNT-like modified probes with abundant nanosized surface structures result in the obviously enhancement of light scattering, which will be detrimental to s-SNOM detection. Therefore, it is necessary to seek a method to further improve the performance of the graphene-coated dielectric probe. Thus, the goal of our next generation probe is to achieve a breakthrough in the preparation and performance of graphene isolation ultra-sharp probe on the surface of dielectric without IR phonon vibration (such as barium fluoride (BaF_2) and calcium fluoride (CaF_2)).

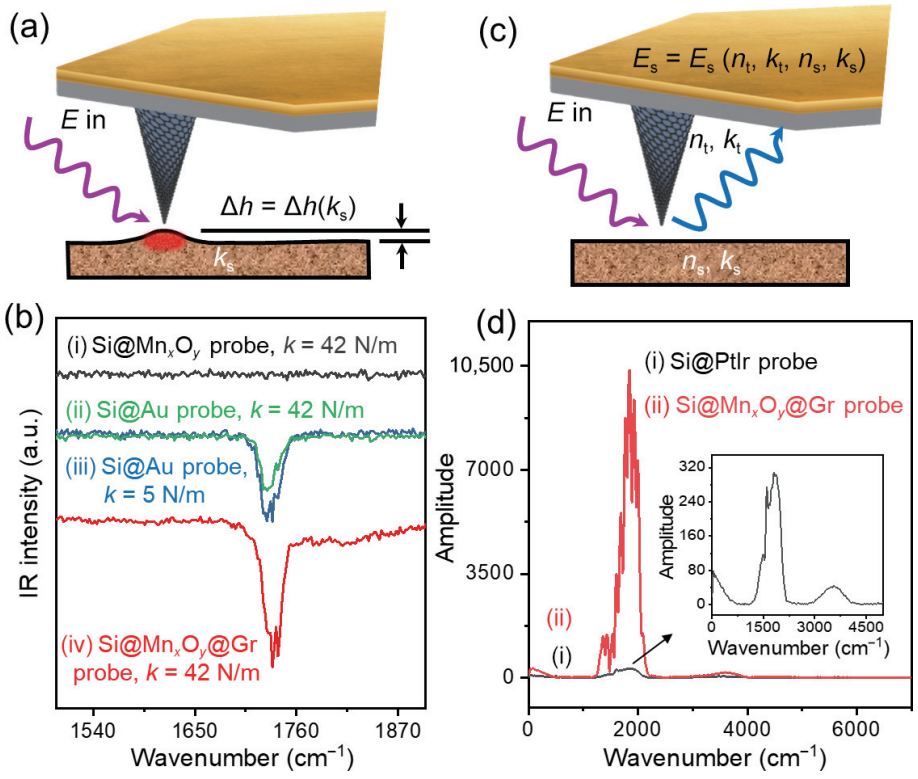

Figure 5 Schematic and corresponding nanoIR properties of graphene-coated dielectric probes. (a) Schematic of the principle of AFM-IR spectroscopy. (b) nanoIR spectra of PMMA standard samples collected by Si@Mn_xO_y probe ((i) k = 42 N/m), Si@Au probe ((ii) k = 42 N/m), commercial Au-coated probe ((iii) HQ:NSC14/Cr-Au, Mikromasch, k = 5 N/m), and Si@Mn_xO_y@Gr probe ((iv) k = 42 N/m), respectively. (c) Schematic of the principle of s-SNOM. (d) Background light scattering of Si substrate tested by commercial PtIr-coated probe ((i) Si@PtIr probe, SCM-PIT-V2, Bruker) and (ii) Si@Mn_xO_y@Gr probe, respectively. The lower right inset shows the zoom-in of (d)(i).

4 Conclusions

In conclusion, we have demonstrated a novel method for achieving continuous single-layer graphene growth on non-planar and amorphous dielectric probe surfaces using MnO-STCVD. The resulting graphene-coated dielectric probes exhibit an average IR reflectance of only 5% in the mid-IR band, which is significantly better than that of probes without continuous graphene coating. These probes effectively transduce the local photothermal sample expansion caused by IR laser pulses and scatter near-field light 25 times more strongly than commercial metal-coated probes, offering advantages in nanoIR sensing based on AFM-IR and IR s-SNOM principles. Our study contributes to the development of new and improved nanoscale probes and provides a platform for exploring new applications of graphene in IR photonics and nanoscale spectroscopy. Moreover, our method offers a solution for growing high-quality graphene on non-planar dielectric materials, which has broad implications for various fields, including integrated circuits and photodetector.

Acknowledgements

This work was financially supported by the National Natural Science Foundation of China (Nos. 22002127, 22275155, 22272140, 22202162, and 21904112), the Natural Science Foundation of Xiamen, China (No. 3502Z20227008), the Fundamental Research Funds for the Central Universities (No. 20720210016), the Ministry of Science and Technology of China, National Key Research and Development Program of China (No. 2021YFA1201502), the Fundamental Research Funds for the Central Universities (No. 20720220011), and China Postdoctoral Science Foundation (No. 2022M722648).

Electronic Supplementary Material: Supplementary material (SEM measurements, AFM imaging, Raman spectroscopy measurements, and summarized data of probes) is available in the online version of this article at https://doi.org/10.1007/s12274-023-5934-1.

References

[1] Dazzi, A.; Prater, C. B. AFM-IR: Technology and applications in nanoscale infrared spectroscopy and chemical imaging. *Chem. Rev.* **2017**, *117*, 5146–5173.

[2] Wang, H. L.; You, E. M.; Panneerselvam, R.; Ding, S. Y.; Tian, Z. Q. Advances of surface-enhanced Raman and IR spectroscopies: From nano/microstructures to macro-optical design. *Light Sci. Appl.* **2021**, *10*, 161.

[3] Rao, V. J.; Matthiesen, M.; Goetz, K. P.; Huck, C.; Yim, C.; Siris, R.; Han, J.; Hahn, S.; Bunz, U. H. F.; Dreuw, A.; et al. AFM-IR and IR-SNOM for the characterization of small molecule organic semiconductors. *J. Phys. Chem. C* **2020**, *124*, 5331–5344.

[4] Mauser, N. and Hartschuh, A. Tip-enhanced near-field optical microscopy. *Chem. Soc. Rev* **2014**, *43*, 1248–1262.

[5] Moore, S. L.; Ciccarino, C. J.; Halbertal, D.; McGilly, L. J.; Finney, N. R.; Yao, K.; Shao, Y.; Ni, G.; Sternbach, A.; Telford, E. J. et al. Nanoscale lattice dynamics in hexagonal boron nitride moiré superlattices. *Nat. Commun.* **2021**, *12*, 5741.

[6] Qi, X. Q.; Lu, Z. H.; You, E. M.; He, Y.; Zhang, Q. E.; Yi, H. J.; Li, D. Y.; Ding, S. Y.; Jiang, Y.; Xiong, X. P. et al. Nanocombing effect leads to nanowire-based, in-plane, uniaxial thin films. *ACS Nano* **2018**, *12*, 12701–12712.

[7] Qin, T. X.; You, E. M.; Zhang, M. X.; Zheng, P.; Huang, X. F.; Ding, S. Y.; Mao, B. W.; Tian, Z. Q. Quantification of electron accumulation at grain boundaries in perovskite polycrystalline films by correlative infrared-spectroscopic nanoimaging and kelvin probe force microscopy. *Light Sci. Appl.* **2021**, *10*, 84.

[8] You, E. M.; Chen, Y. Q.; Yi, J.; Meng, Z. D.; Chen, Q.; Ding, S. Y.; Duan, H. G.; Moskovits, M.; Tian, Z. Q. Nanobridged rhombic

antennas supporting both dipolar and high-order plasmonic modes with spatially superimposed hotspots in the mid-infrared. *Opto-Electron. Adv.* **2021**, *4*, 210076.

[9] Schwartz, J. J.; Jakob, D. S.; Centrone, A. A guide to nanoscale IR spectroscopy: Resonance enhanced transduction in contact and tapping mode AFM-IR. *Chem. Soc. Rev.* **2022**, *51*, 5248–5267.

[10] Guo, Q. S.; Li, C.; Deng, B. C.; Yuan, S. F.; Guinea, F.; Xia, F. N. Infrared nanophotonics based on graphene plasmonics. *ACS Photonics* **2017**, *4*, 2989–2999.

[11] Low, T.; Chaves, A.; Caldwell, J. D.; Kumar, A.; Fang, N. X.; Avouris, P.; Heinz, T. F.; Guinea, F.; Martin-Moreno, L.; Koppens, F. Polaritons in layered two-dimensional materials. *Nat. Mater.* **2017**, *16*, 182–194.

[12] Maier, S. A. *Plasmonics*: *Fundamentals and Applications*; Springer: New York, 2007.

[13] Koppens, F. H. L.; Chang, D. E.; García De Abajo, F. J. Graphene plasmonics: A platform for strong light–matter interactions. *Nano Lett.* **2011**, *11*, 3370–3377.

[14] Lu, W. B.; Zhu, W.; Xu, H. J.; Ni, Z. H.; Dong, Z. G.; Cui, T. J. Flexible transformation plasmonics using graphene. *Opt. Express* **2013**, *21*, 10475–10482.

[15] Zhu, B. F.; Ren, G. B.; Gao, Y. X.; Yang, Y.; Lian, Y. D.; Jian, S. S. Graphene-coated tapered nanowire infrared probe: A comparison with metal-coated probes. *Opt. Express* **2014**, *22*, 24096–24103.

[16] Hui, F.; Chen, S. C.; Liang, X. H.; Yuan, B.; Jing, X.; Shi, Y. Y.; Lanza, M. Graphene coated nanoprobes: A review. *Crystals* **2017**, *7*, 269.

[17] Hui, F.; Vajha, P.; Shi, Y. Y.; Ji, Y. F.; Duan, H. L.; Padovani, A.; Larcher, L.; Li, X. R.; Xu, J. J.; Lanza, M. Moving graphene devices from lab to market: Advanced graphene-coated nanoprobes. *Nanoscale* **2016**, *8*, 8466–8473.

[18] Lanza, M.; Bayerl, A.; Gao, T.; Porti, M.; Nafria, M.; Jing, G. Y.; Zhang, Y. F.; Liu, Z. F.; Duan, H. L. Graphene-coated atomic force microscope tips for reliable nanoscale electrical characterization. *Adv. Mater.* **2013**, *25*, 1440–1444.

[19] Martin-Olmos, C.; Rasool, H. I.; Weiller, B. H.; Gimzewski, J. K. Graphene MEMS: AFM probe performance improvement. *ACS Nano* **2013**, *7*, 4164–4170.

[20] Wang, Z. W.; Xue, Z. Y.; Zhang, M.; Wang, Y. Q.; Xie, X. M.; Chu, P. K.; Zhou, P.; Di, Z. F.; Wang, X. Germanium-assisted direct growth of graphene on arbitrary dielectric substrates for heating devices. *Small* **2017**, *13*, 1700929.

[21] Khan, A.; Islam, S. M.; Ahmed, S.; Kumar, R. R.; Habib, M. R.; Huang, K.; Hu, M.; Yu, X. G.; Yang, D. R. Direct CVD growth of graphene on technologically important dielectric and semiconducting substrates. *Adv. Sci.* **2018**, *5*, 1800050.

[22] Chen, K.; Zhou, X.; Cheng, X.; Qiao, R. X.; Cheng, Y.; Liu, C.; Xie, Y. D.; Yu, W. T.; Yao, F. R.; Sun, Z. P. et al. Graphene photonic crystal fibre with strong and tunable light–matter interaction. *Nat. Photonics* **2019**, *13*, 754–759.

[23] Xia-Hou, Y. J.; Yu, Y.; Zheng, J. R.; Yi, J.; Zhou, J.; Qin, T. X.; You, E. M.; Chen, H. L.; Ding, S. Y.; Zhang, L. et al. Graphene coated dielectric hierarchical nanostructures for highly sensitive broadband infrared sensing. *Small* **2023**, *19*, 2206167.

[24] Ferrari, A. C.; Robertson, J. Interpretation of Raman spectra of disordered and amorphous carbon. *Phys. Rev. B* **2000**, *61*, 14095–14107.

[25] Luong, D. X.; Bets, K. V.; Algozeeb, W. A.; Stanford, M. G.; Kittrell, C.; Chen, W. Y.; Salvatierra, R. V.; Ren, M. Q.; McHugh, E. A.; Advincula, P. A. et al. Gram-scale bottom-up flash graphene synthesis. *Nature* **2020**, *577*, 647–651.

[26] Bachmatiuk, A.; Mendes, R. G.; Hirsch, C.; Jähne, C.; Lohe, M. R.; Grothe, J.; Kaskel, S.; Fu, L.; Klingeler, R.; Eckert, J. et al. Few-layer graphene shells and nonmagnetic encapsulates: A versatile and nontoxic carbon nanomaterial. *ACS Nano* **2013**, *7*, 10552–10562.

[27] Rümmeli, M. H.; Kramberger, C.; Grüneis, A.; Ayala, P.; Gemming, T.; Büchner, B.; Pichler, T. On the graphitization nature of oxides for the formation of carbon nanostructures. *Chem. Mater.* **2007**, *19*, 4105–4107.

[28] Zou, Z. Y.; Fu, L.; Song, X. J.; Zhang, Y. F.; Liu, Z. F. Carbide-forming groups IVB-VIB metals: A new territory in the periodic table for CVD growth of graphene. *Nano Lett.* **2014**, *14*, 3832–3839.

[29] Chen, K.; Zhang, F.; Sun, J. Y.; Li, Z. Z.; Zhang, L.; Bachmatiuk, A.; Zou, Z. Y.; Chen, Z. L.; Zhang, L. Y.; Rümmeli, M. H. et al. Growth of defect-engineered graphene on manganese oxides for Li-ion storage. *Energy Storage Mater.* **2018**, *12*, 110–118.

[30] Cocker, T. L.; Jelic, V.; Hillenbrand, R.; Hegmann, F. A. Nanoscale terahertz scanning probe microscopy. *Nat. Photonics* **2021**, *15*, 558–569.

[31] Li, Z. Q.; Lu, C. J.; Xia, Z. P.; Zhou, Y.; Luo, Z. X-ray diffraction patterns of graphite and turbostratic carbon. *Carbon* **2007**, *45*, 1686–1695.

[32] Kumar, R.; Oh, J. H.; Kim, H. J.; Jung, J. H.; Jung, C. H.; Hong, W. G.; Kim, H. J.; Park, J. Y.; Oh, I. K. Nanohole-structured and palladium-embedded 3D porous graphene for ultrahigh hydrogen storage and CO oxidation multifunctionalities. *ACS Nano* **2015**, *9*, 7343–7351.

[33] Yasuda, A. A new technique using FT-IR micro-reflectance spectroscopy for measurement of water concentrations in melt inclusions. *Earth Planets Space* **2014**, *66*, 34.

[34] Azarfar, G.; Aboualizadeh, E.; Walter, N. M.; Ratti, S.; Olivieri, C.; Norici, A.; Nasse, M.; Kohler, A.; Giordano, M.; Hirschmugl, C. J. Estimating and correcting interference fringes in infrared spectra in infrared hyperspectral imaging. *Analyst* **2018**, *143*, 4674–4683.